

Pulsed quantum-cascade laser-based sensor for trace-gas detection of carbonyl sulfide

Gerard Wysocki, Matt McCurdy, Stephen So, Damien Weidmann, Chad Roller, Robert F. Curl, and Frank K. Tittel

Simultaneous exhaled carbonyl sulfide (OCS) and carbon dioxide concentration measurements in human breath are demonstrated with a compact pulsed quantum-cascade laser-based gas sensor. We achieved a noise-equivalent sensitivity (1σ) of 1.2 parts per billion by measuring a well-isolated OCS $P(11)$ absorption line in the ν_3 band at 2057.6 cm^{-1} using an astigmatic Herriott cell of 36-m optical path length and 0.4-s acquisition time. © 2004 Optical Society of America

OCIS codes: 300.1030, 280.3420.

1. Introduction

Detection and analysis of carbonyl sulfide (OCS) is of importance in a number of applications that include medical diagnostics, atmospheric chemistry,^{1,2} and industrial emission monitoring (natural gas quality evaluation).³ Elevated OCS concentrations in exhaled breath have been reported in lung transplant recipients suffering from acute rejection⁴ as well as in patients with liver disease.⁵ The low parts per billion (ppb) concentration range of many volatile molecular species in human breath presents a complex challenge for clinical breath analysis applications, which require rapid *in situ* detection of trace gases. In this context, rapid analysis of expired breath by use of mid-IR laser absorption spectroscopy is a desirable noninvasive alternative to the currently used invasive diagnostic methods (e.g., bronchoscopic lung biopsies to assess lung transplant acute rejection). This technique does not require the sample preparation or preconcentration techniques associated with gas chromatography, which is the most frequently used method for trace detection of sulfur compounds.^{6–8} In terms of previous mid-IR methods used to measure OCS concentrations at trace gas levels, Fried *et al.*⁹ have measured low ambient con-

centration of OCS [~ 500 parts per trillion (ppt)] with a precision of less than 5 ppt using mid-IR laser absorption spectroscopy based on a cryogenically cooled, cw, lead salt diode laser with a $2f$ detection scheme, a path length of 117 m, and a data-acquisition integration time of 2 min. Quantum-cascade lasers (QCLs) have the advantage of operating within thermoelectric cooling ranges with minimal component requirements and are efficient, robust, and reliable mid-IR sources.¹⁰ Their characteristics permit the design of a selective, sensitive, compact, and liquid-nitrogen-free trace-gas sensor suitable for clinical or field applications.

In this paper we report on the development and evaluation of an advanced design of a mid-IR laser absorption spectroscopy-based OCS sensor utilizing a thermoelectrically cooled, pulsed QCL. We improved the detection sensitivity of the sensor by more than 1 order of magnitude in comparison with the previously reported performance in Ref. 11 by applying fast wavelength scanning as well as improved data acquisition and processing techniques, which result in better noise cancellation.

2. Experimental Details

A. System Configuration

The sensor architecture is schematically shown in Fig. 1. A thermoelectrically cooled pulsed distributed feedback QCL was placed inside a vacuum-tight laser housing. The wavelength of the laser can be tuned thermally between 2054.5 and 2060.5 cm^{-1} by a change in the temperature of the QCL chip from $-36\text{ }^\circ\text{C}$ to $+10\text{ }^\circ\text{C}$. Absorption features of several molecules such as OCS, CO_2 , H_2O , and CO are within

The authors are with the Department of Electrical and Computer Engineering, Rice University, 6100 Main Street, Houston, Texas 77251. The e-mail address for G. Wysocki is gerardw@rice.edu.

Received 19 March 2004; revised manuscript received 12 July 2004; accepted 27 July 2004.

0003-6935/04/326040-07\$15.00/0

© 2004 Optical Society of America

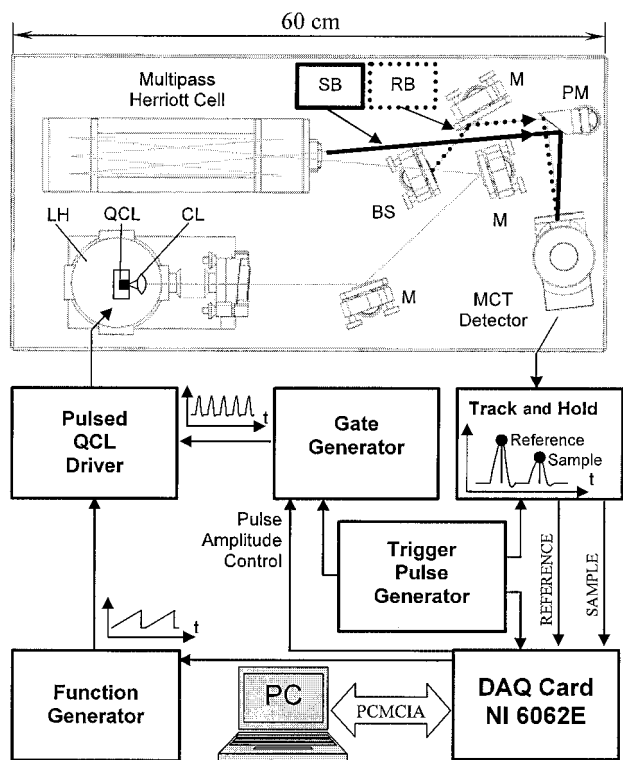


Fig. 1. Schematic configuration of the QCL-based gas sensor. QCL, quantum cascade laser chip; LH, laser housing; CL, collimating lens; SB, sample beam; RB, reference beam; M, mirror; BS, beam splitter; PM, off-axis parabolic mirror; MCT, mercury cadmium telluride; DAQ, data acquisition.

the tuning range of this laser and can be used for chemical sensing applications. To perform fast frequency scanning, a sawtooth waveform was applied to the QCL, thereby modulating the subthreshold laser current at a fixed operating temperature of the QCL heat sink.¹² The laser was supplied with ~ 25 -ns injection current pulses at a repetition rate of 125 kHz with the maximum frequency limited by the sampling rate of the data-acquisition electronics. The measurement method applied in this experiment employs dual-channel (sample and reference) data acquisition with a single detector.^{13,14} The reference channel is important for spectroscopic applications in which pulsed QCLs are used because pulse-to-pulse fluctuations of the laser optical power degrade the signal-to-noise ratio (SNR) of the measured absorption data. After collimation by an antireflection-coated ZnSe aspherical lens with a 3-mm focal length and a 6-mm diameter located inside the laser housing, the laser beam is divided into sample and reference beams in the ratio of 2 to 1, respectively, with a ZnSe beam splitter as shown in Fig. 1. The sample beam passes through the multipass astigmatic Herriott cell (New Focus, Model 5611) with a 36-m optical path length and, upon exiting, is focused on a fast (50-MHz bandwidth) mercury cadmium telluride detector (Kolmar Technologies Inc., Model KMPV8-1-J1) by an off-axis parabolic mirror. The reference beam is directed onto the same detector. Because of

the difference in the optical path length between the channels, the sample optical pulse arrives approximately 120 ns later than the reference pulse. We use fast track-and-hold electronics with a 350-MHz sampling bandwidth and a 125-MHz maximum sampling rate (Analog Devices, Model AD9101) for a time-resolved capture of the peak optical intensity of the sample and reference laser pulses. Track-and-hold electronics operate as an analog buffer, which can retain an acquired voltage value as long as necessary for successive digitization with an analog-to-digital converter. The sampling rate of the analog-to-digital converter becomes the limiting factor of the time-resolved system performance. For this study data acquisition and processing were performed by a laptop computer equipped with a 500-kilosample/s PCMCIA data-acquisition card (National Instruments, Model DAQ 6062E). The overall system synchronization and pulse train generation are performed by an external four-channel pulse generator (Berkeley Nucleonics Corporation, Model 555).

B. Carbonyl Sulfide Spectral Line Selection

The measurement of low OCS concentrations (i.e., ppb levels) in human breath requires selection of the optimum spectroscopic line available in the spectral range of the QCL. The line selected should satisfy the following conditions: (1) good line intensity, (2) minimal spectral interference by nearby CO_2 and H_2O absorption lines, and (3) the availability of a neighboring CO_2 line within the fast tuning range of the QCL for ventilation monitoring simultaneously with a OCS measurement. Simultaneous measurement of exhaled CO_2 is needed to verify correct breath donations, to normalize the resulting OCS concentrations, and to standardize measurement conditions.^{15,16}

Figure 2 shows OCS and CO_2 spectral lines in the region of the OCS $P(11)$ line simulated for expected operating conditions by use of the HITRAN 2000 database.¹⁷ Initially two OCS spectral features in its ν_3 band were considered: $P(14)$ (line strength of $8.82 \times 10^{-19} \text{ cm}^{-1} \text{ molecule cm}^{-2}$) and $P(11)$ (line strength of $7.49 \times 10^{-19} \text{ cm}^{-1} \text{ molecule cm}^{-2}$). However, for breath samples with elevated CO_2 levels (above $\sim 4\%$), we observed strong spectral wing contributions from $P(26)$ of the $\text{CO}_2 \nu_1 + \nu_2$ band to the OCS $P(14)$ line. We ascertained that low OCS concentrations can be measured more accurately with an $\sim 15\%$ weaker OCS $P(11)$ line. The $P(49)$ line of the $\text{CO}_2 \nu_1 + 2\nu_2 - \nu_2$ band can be used to monitor exhaled CO_2 . For more accurate concentration measurements of CO_2 , the influence of the neighboring OCS $P(12)$ line can be eliminated by subtraction of the OCS spectrum calculated from the concentration measured with the OCS $P(11)$ line.

A gas cell pressure of 60 Torr was chosen. It is sufficiently low to assure a satisfactory separation of the OCS $P(12)$ and $\text{CO}_2 P(49)$ lines as well as to minimize any contribution of wing effects from strong $\nu_1 + \nu_2$ CO_2 lines $P(24)$ and $P(26)$, which can affect the OCS measurement at line $P(11)$.

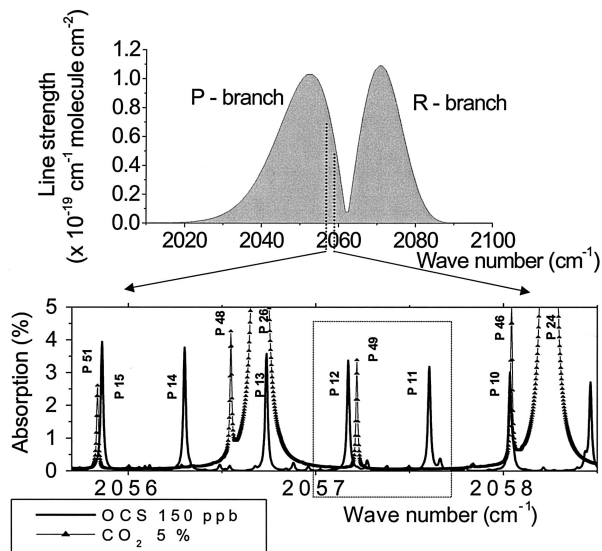


Fig. 2. Simulated OCS spectrum (HITRAN 2000). Upper plot shows absorption line strengths in the OCS fundamental rovibrational spectrum. The region of interest is shown in the lower plot of absorption spectra of OCS and CO₂ simulated for assumed operating conditions (pressure, 60 Torr; optical path length, 36 m; OCS concentration, 150 ppb; and CO₂ concentration, 5%).

C. Optimization of Laser Parameters

The laser linewidths of the QCLs operated in pulsed mode are broadened by the frequency chirping associated with temperature effects in the laser structure.¹⁸ These effects become more pronounced for long pulse durations or high peak current pulses. To optimize the laser operating parameters, the laser linewidth was analyzed at different amplitudes of the 25-ns laser current pulses at a 125-kHz repetition rate. We performed these measurements, presented in Fig. 3(a), by scanning the laser line over a Doppler-limited OCS *P*(11) line from a 1.6-parts per million (ppm) OCS sample at low pressure (1.2 Torr). The Doppler linewidth of OCS calculated at room temperature is 0.003 cm⁻¹, which is at least 1 order of magnitude smaller than the full width at half-maximum (FWHM) of the observed instrument response. Thus the observed line can essentially be considered the laser spectral envelope. The laser linewidth increases with increasing amplitude of the pump current pulses. This effect reduces the spectral selectivity of the gas sensor, which is shown in Fig. 3(b) as a ratio of the molecular linewidth of OCS at the set working pressure (60 Torr) and the QCL linewidth (FWHM_{OCS}/FWHM_{QCL}). Simultaneously, increasing the optical peak power of the laser causes a reduction of the noise level present in the derived absorption spectrum. This effect improves the SNR and thus translates into lower minimum detectable concentrations. The SNR of the spectrum can be characterized by the ratio of absorption peak amplitude A_{PEAK} to the standard deviation of the noise σ_{NOISE} . Figure 3(b) shows the effect of laser power on the SNR of the sensor and indicates the limitation due to the noise level of the detection system. The

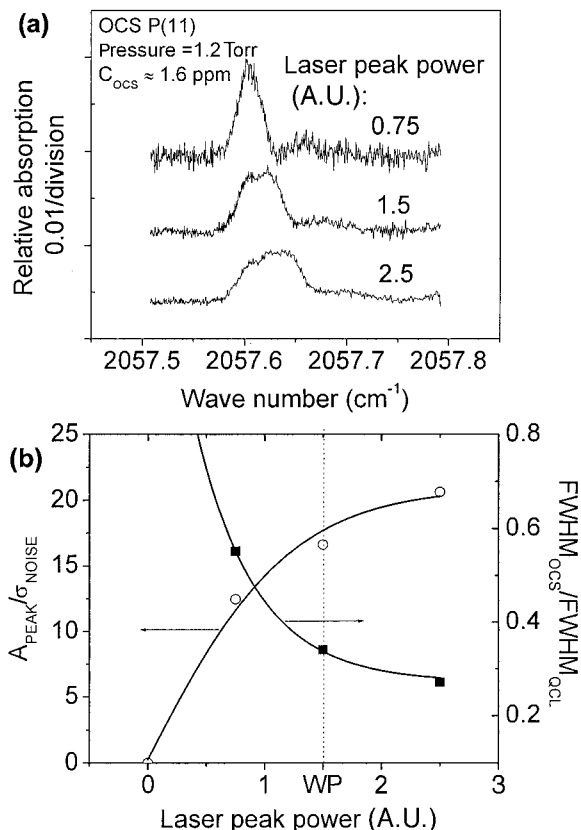


Fig. 3. (a) Relative absorption in a low-pressure (1.2-Torr) OCS sample as a function of wavelength depicting the QCL linewidth for three different optical power levels. (b) Spectral SNR, $A_{\text{PEAK}}/\sigma_{\text{NOISE}}$, and sensor selectivity $\text{FWHM}_{\text{OCS}}/\text{FWHM}_{\text{QCL}}$ versus laser peak power. WP, working point chosen for experimental measurements.

selected OCS line is well isolated from other spectral lines. Thus the spectral resolution of the sensor is not critical. In this case we found a compromise by operating the laser at an intermediate power level corresponding to a 1.5-V reference signal peak amplitude [a value of the detector output signal amplified four times by the track-and-hold circuit indicated in Fig. 3(b) as a working point], which assures sufficient selectivity and maximum sensitivity of the sensor system.

The dependence of the laser power on the operating temperature together with a relatively long time constant for charging energy storage capacitors in the laser current driver (Directed Energy Inc., Model DLD-100B) produce variations of laser power during the modulation of the laser bias. Figure 4(a) shows a plot of the behavior of laser power over one cycle of the applied subthreshold current ramp waveform for frequency scanning. As discussed above, the spectral noise is inversely proportional to the laser power, resulting in increased noise levels at the end of the frequency scan where the power decreased [see the inserted dotted box in the measured spectrum of 50-ppb OCS depicted in Fig. 4(a)]. This phenomenon limits the effective range of the frequency scan to the region where the noise is relatively small in compar-

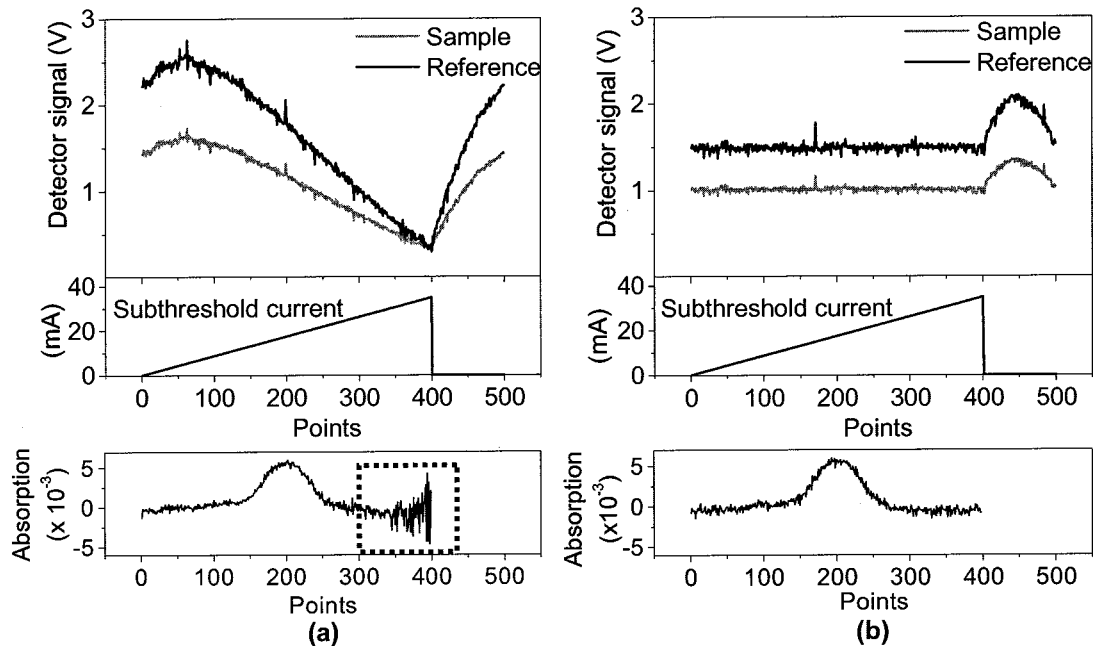


Fig. 4. (a) Laser power fluctuations (upper plot) produced with laser frequency scanning by subthreshold current modulation and an example of the resulting noise level in a spectrum of a 50-ppb OCS in a N_2 mixture measured by the data-acquisition system (the x scale shows a relative number of points in the scan). (b) The same as (a) but with an applied laser-pulse amplitude modulation technique. Stabilization occurs only during the slope of the subthreshold current waveform in the range between 1 and 400 points. The laser power is not stabilized during the flat part of the waveform between 400 and 500 points, which is visible as a protrusion in the upper plot depicting the laser power behavior.

ison with the height of a spectral absorption line. To avoid these limitations, an amplitude modulation of the laser current pulses was applied. To do this, we recorded the shape of the optical power fluctuations resulting from the wavelength tuning process using the reference channel. From the results of these measurements, a correction signal was calculated and then applied to the laser as a pulse amplitude modulation waveform by means of a digital-to-analog converter. This operation stabilizes the laser power during a frequency scan as shown in Fig. 4(b). As a consequence, the noise level in the measured spectrum of 50-ppb OCS in Fig. 4(b) remains constant over the entire scan range.

D. Gas Sensor Calibration

The QCL was biased with a subthreshold current sawtooth waveform at a frequency of 250 Hz and with an ~ 35 -mA peak-to-peak amplitude, which provides complete coverage of the measured spectral lines. We generated this waveform by using an external synchronized function generator (Stanford Research Systems, Model DS345). We performed the calibration of the frequency scans using an etalon that consists of two ZnSe wedged windows separated by 18.5 cm, resulting in a free spectral range of 0.027 cm^{-1} . Figure 5 shows a frequency calibration curve fitted by a second-order polynomial function. To increase the number of data points in the calibration curve, we utilized the positions of both the minima and the

maxima of the etalon fringe pattern. The full range of a single frequency scan covered $\sim 0.3 \text{ cm}^{-1}$.

We performed the calibration of the OCS concentration measurements and determined the detection limit of the reported sensor using a permeation-tube-based precision gas standard generator (Kin-Tek, Model 491M). To determine the concentration C of OCS in an unknown gas sample, a fitting procedure was applied to the measured spectrum $g_{\text{meas}}(\nu)$ by a predefined tabulated reference spectrum $g_{\text{ref}}(\nu)$ measured for a sample of known concentration C_{ref} .¹⁹ Both measurements were carried out at the same

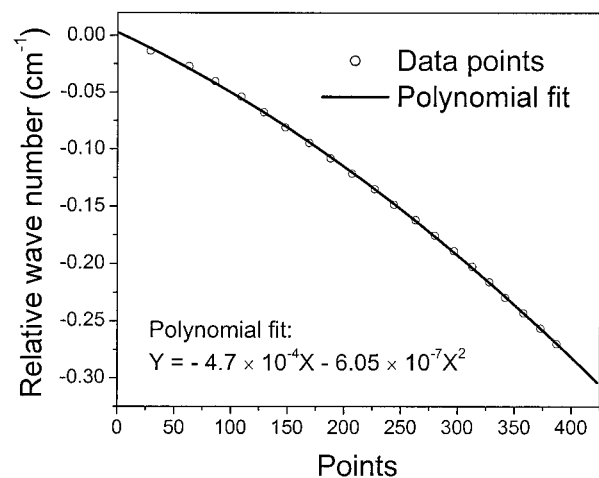


Fig. 5. Calibration curve of the QCL frequency scan.

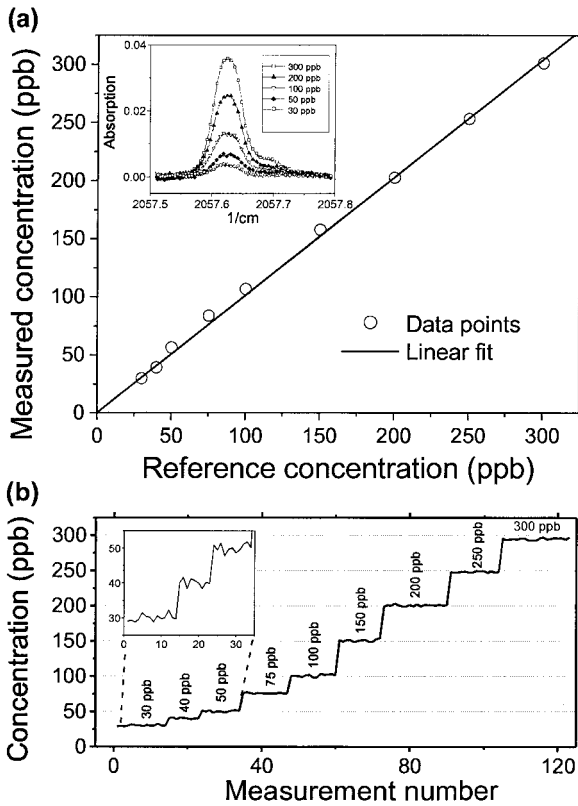


Fig. 6. (a) Calibration curve for OCS concentration measurements together with five examples of measured spectra (see inset) obtained with a precision gas standard generator. (b) OCS concentration calculated in quasi-real-time by a linear fitting procedure for measured spectra with 100 averaged scans.

conditions. The slope $tg(\alpha)$ of a linear regression fit of the function $g_{\text{meas}}(\nu) = f[g_{\text{ref}}(\nu)]$ yields the ratio of concentrations C/C_{ref} . The linearity of the sensor response is presented in Fig. 6(a), which depicts the measured concentration as a function of the reference mixture concentration produced by the gas standard generator. Each data point in this plot was determined by a linear least-squares fit of the measured 400-point spectrum (1000 averaged scans and 4-s acquisition time) with the reference spectrum. A 300-ppb OCS in a N_2 mixture was used for the reference spectrum, which was measured with the same conditions as the sample spectrum and smoothed by a degree 2 Savitzky–Golay 41-point filter. The above-mentioned fitting algorithm can be implemented for a quasi-real-time measurement. A concentration plot shown in Fig. 6(b) was recorded by this technique. We derived each data point in this plot utilizing post-processing of the 100 averages of 400-point scans (acquisition time of 0.4 s). The response time of the gas standard generator and the pumping system are relatively slow; thus the data acquisition was performed only when the set concentration achieved a steady state.

To estimate the minimum detection limit of the sensor, the relationship between the standard deviation of the absorption line fit residual σ and the

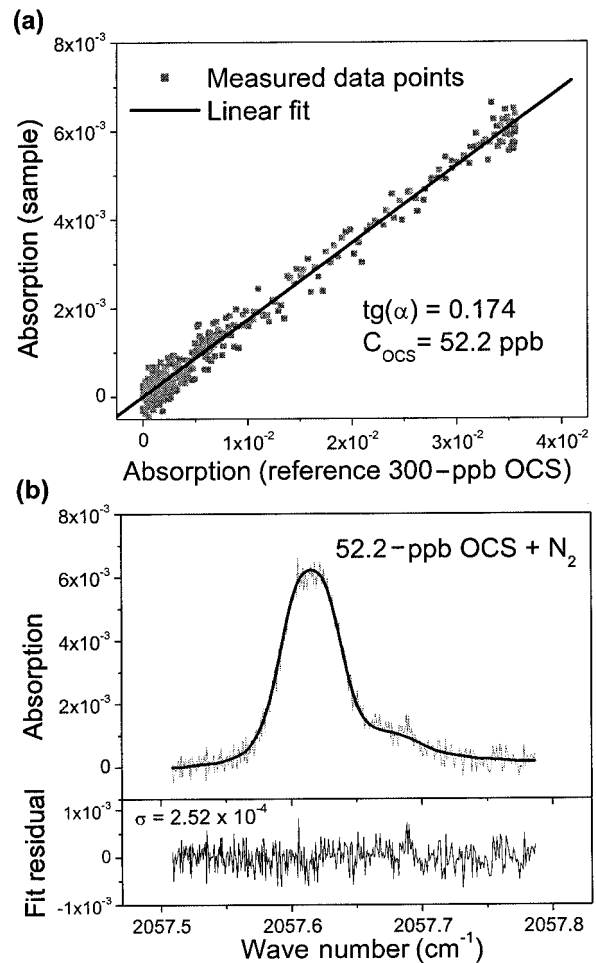


Fig. 7. (a) Concentration measurement from a linear regression fit and (b) acquired spectrum of 52.2 ppb of OCS in a N_2 mixture depicting a noise-equivalent sensitivity estimate.

standard error δA_L in the integrated absorption line intensity A_L , which is $\delta A_L = \sigma[\Delta\nu/\int g^2(\nu)d\nu]^{1/2}$, was used.²⁰ Here $\Delta\nu$ denotes the average point spacing in the frequency scale, which in our case is $\sim 0.705 \times 10^{-3} \text{ cm}^{-1}$, and $g(\nu)$ represents the line profile of the reference spectrum normalized by the condition $\int g(\nu)d\nu = 1$. We recorded a 400-point spectrum of a 52.2-ppb OCS in a N_2 gas sample shown in Fig. 7(b) using 1000 averaged scans acquired within 4 s. This spectrum was also fitted with a reference spectrum of 300-ppb OCS as described above [see Fig. 7(a)]. The standard deviation of the fit residual, $\sigma = 2.52 \times 10^{-4}$; the area under the spectral line, $A_L = 4.3 \times 10^{-4} \text{ cm}^{-1}$; and the integral, $\int g^2(\nu)d\nu = 9.27 \text{ cm}$, yield the minimum detection limit of $C(1\sigma) = (\delta A_L/A_L) 52.2 \text{ ppb} \approx 0.27 \text{ ppb}$. This equation is valid only for uncorrelated noise at every spectral point and therefore does not take into account possible baseline fluctuations. The data presented in Fig. 6(b) allow us to evaluate the actual sensor performance. Each point in this plot is a result of our averaging 100 scans; therefore the precision calculated with this equation is $0.27 \text{ ppb} (1000/100)^{1/2} = 0.85 \text{ ppb}$. The standard deviation calculated directly from the scattering of the

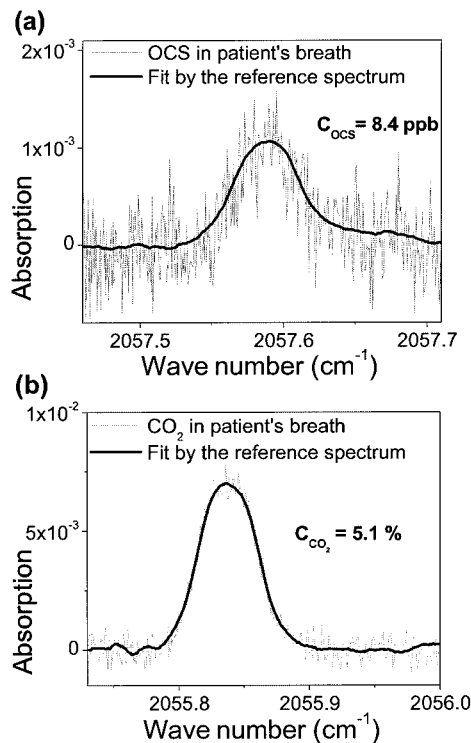


Fig. 8. Measured spectra and calculated concentrations of (a) OCS and (b) CO_2 in a breath sample of a lung transplant recipient. [The baseline was fitted in the frequency range on each side of the absorption line and subtracted to create plot (a)].

concentration measurements in Fig. 6(b) is 1.2 ppb. Thus nonstatistical factors such as baseline variations introduce only moderate additional noise, and the sensor performance is primarily limited by the noise of detectors and sampling electronics.

E. Measurements of Breath Samples

The QCL-based sensor was used to measure OCS concentration in human breath samples taken from lung transplant recipients. This kind of analysis was previously demonstrated with gas chromatography.^{4,5,21} Sampling was performed with chemically inert 1-l Tedlar sampling bags (SKC Incorporated). Samples were analyzed within 2 h after collection. A small portion of the gas sample was injected into the initially evacuated multipass cell, and its spectrum was measured at a total pressure of 60 Torr. Figure 8 shows an example measurement of a sample taken from a lung transplant patient with suspected bronchiolitis. Figure 8(a) shows the OCS spectrum fitted with a tabulated reference spectrum recorded with 50-ppb OCS in a N_2 mixture. The OCS concentration detected in this sample was estimated to be at the ~ 8.4 -ppb level.

The same measurement method is applied to detect CO_2 in a patient's breath. In this case a CO_2 measurement was performed with the CO_2 $P(51)$ spectral line at 2055.837 cm^{-1} [see Fig. 8(b)]. A CO_2 concentration of $\sim 5.1\%$ was determined on the basis of a comparison with the spectrum of a 5% CO_2 in an air

reference mixture. As discussed above, the current sensor uses the neighboring 30% stronger CO_2 $P(49)$ line for the measurement of CO_2 . In this case, we performed the switching between the required wavelengths using the dc level of the laser bias without changing the working temperature of the laser heat sink. This simplifies the operation of the sensor, which significantly increases its functionality and reduces the influence of human operating factors. This is an important consideration in potential medical applications.

3. Conclusions

An OCS trace-gas sensor platform based on a direct mid-IR laser absorption measurement technique with a pulsed QCL and a compact 36-m multipass cell with a minimum detection limit, $C(1\sigma)$, of 1.2 ppb (for 100 averaged 400-point frequency scans acquired within ~ 0.4 s) was developed and demonstrated. Such a precision makes the reported sensor capable of detecting OCS levels that are elevated only four times above typical atmospheric concentrations (~ 500 ppt),¹ which must be considered as the background concentration for OCS analysis in human breath.

An off-line analysis of human breath samples from lung transplant recipients demonstrated the feasibility of concentration measurement of low ppb OCS levels, as well as the multispecies (OCS and CO_2) detection capability of a QCL-based breath analyzer.

Several further system performance improvements can be implemented such as use of a QCL, which can access the OCS $R(23)$ spectral line in the ν_3 band at 2071.206 cm^{-1} . This absorption is also free of interfering gas species as the $P(11)$ line used in this study but offers a 40% stronger absorption line intensity. A further future development for an advanced laser-based gas sensor is to upgrade the current data-acquisition system with digital-signal-processing-based technology to implement high-resolution, real-time trace gas monitoring, such as in biomedical diagnostics (e.g., on-line breath analysis) and environmental and industrial emission monitoring.³ Such a potential sensor enhancement scheme will result in faster statistical noise cancellation as well as an improved trace-gas sensor portability.

The authors thank Claire Gmachl (Princeton University, N.J.) and Deborah Sivco (Lucent Technologies, Inc., N.J.) for providing us with the QCL used in this study, Remzi Bag and Carolyn M. Paraguaya (Baylor College of Medicine, Houston, Tex.) for supplying breath samples, and Anatoliy Kosterev for useful discussions. The authors also gratefully acknowledge financial support from the Texas Advanced Technology Program, the Robert Welch Foundation, the National Science Foundation, and the U.S. Office of Naval Research through a subaward from Texas A&M University and the National Aeronautics and Space Administration.

References

1. M. Von Hobe, G. A. Cutter, A. J. Kettle, and M. O. Andreae, "Dark production: a significant source of oceanic OCS," *J. Geophys. Res.* **106C**, 31217–31226 (2001).
2. A. J. Kettle, U. Kuhn, M. von Hobe, J. Kesselmeier, and M. O. Andreae, "Global budget of atmospheric carbonyl sulfide: temporal and spatial variations of the dominant sources and sinks," *J. Geophys. Res.* **107D**, 25-1–25-16 (2002).
3. P. D. N. Svoronos and T. J. Bruno, "Carbonyl sulfide: a review of its chemistry and properties," *Ind. Eng. Chem. Res.* **41**, 5321–5336 (2002).
4. S. M. Studer, J. B. Orens, I. Rosas, J. A. Krishnan, K. A. Cope, S. Yang, J. V. Conte, P. B. Becker, and T. H. Risby, "Patterns and significance of exhaled-breath biomarkers in lung transplant recipients with acute allograft rejection," *J. Heart Lung Transplant* **20**, 1158–1166 (2001).
5. S. S. Sehnert, L. Jiang, J. F. Burdick, and T. H. Risby, "Breath biomarkers for detection of human liver diseases: preliminary study," *Biomarkers* **7**, 174–187 (2002).
6. P. A. Steudler and W. Kijowski, "Determination of reduced sulfur gases in air by solid absorbent preconcentration and gas chromatography," *Anal. Chem.* **56**, 1432–1436 (1984).
7. W. Wardencki, "Problems with the determination of environmental sulphur compounds by gas chromatography," *J. Chromatog. A* **793**, 1–19 (1998).
8. Y. Inomata, K. Matsunaga, Y. Murai, K. Osada, and Y. Iwasaka, "Simultaneous measurement of volatile sulfur compounds using ascorbic acid for oxidant removal and gas chromatography—flame photometric detection," *J. Chromatog. A* **864**, 111–119 (1999).
9. A. Fried, J. R. Drummond, B. Henry, and J. Fox, "Versatile integrated tunable diode laser system for high precision: application for ambient measurements of OCS," *Appl. Opt.* **30**, 1916–1932 (1991).
10. A. A. Kosterev and F. K. Tittel, "Chemical sensors based on quantum cascade lasers," *IEEE J. Quantum Electron.* **38**, 582–591 (2002).
11. C. Roller, A. A. Kosterev, F. K. Tittel, K. Uehara, C. Gmachl, and D. L. Sivco, "Carbonyl sulfide detection with a thermoelectrically cooled mid-infrared quantum cascade laser," *Opt. Lett.* **28**, 2052–2054 (2003).
12. K. Namjou, S. Cai, E. A. Whittaker, J. Faist, C. Gmachl, F. Capasso, D. L. Sivco, and A. Y. Cho, "Sensitive absorption spectroscopy with a room-temperature distributed-feedback quantum-cascade laser," *Opt. Lett.* **23**, 219–221 (1998).
13. D. D. Nelson, J. H. Shorter, J. B. McManus, and M. S. Zahniser, "Sub-part-per-billion detection of nitric oxide in air using a thermoelectrically cooled mid-infrared quantum cascade laser spectrometer," *Appl. Phys. B* **75**, 343–350 (2002).
14. D. Weidmann, A. A. Kosterev, C. Roller, R. F. Curl, M. P. Fraser, and F. K. Tittel, "Monitoring of ethylene by a pulsed quantum cascade laser," *Appl. Opt.* **43**, 3329–3334 (2004).
15. H. C. Niu, D. A. Schoeller, and P. D. Klein, "Improved gas chromatographic quantitation of breath hydrogen by normalization to respiratory carbon dioxide," *J. Lab. Clin. Med.* **94**, 755–763 (1979).
16. C. Roller, K. Namjou, J. D. Jeffers, M. Camp, A. Mock, P. J. McCann, and J. Grego, "Nitric oxide breath testing by tunable-diode laser absorption spectroscopy: application in monitoring respiratory inflammation," *Appl. Opt.* **41**, 6018–6029 (2002).
17. L. S. Rothman, A. Barbe, D. C. Benner, L. R. Brown, C. Camy-Peyret, M. R. Carleer, K. Chance, C. Clerbaux, V. Dana, V. M. Devi, A. Fayt, J.-M. Flaud, R. R. Gamache, A. Goldman, D. Jacquemart, K. W. Jucks, W. J. Lafferty, J.-Y. Mandin, S. T. Massie, V. Nemtchinov, D. A. Newnham, A. Perrin, C. P. Rinsland, J. Schroeder, K. M. Smith, M. A. H. Smith, K. Tang, R. A. Toth, J. Vander Auwera, P. Varanasi, and K. Yoshino, "The HITRAN molecular spectroscopic database: edition of 2000 including updates through 2001," *J. Quant. Spectrosc. Radiat. Transfer* **82**, 5–44 (2003).
18. J. Faist, C. Gmachl, F. Capasso, C. Sirtori, D. L. Sivco, J. N. Baillargeon, and A. Y. Cho, "Distributed feedback quantum cascade lasers," *Appl. Phys. Lett.* **70**, 2670–2672 (1997).
19. A. A. Kosterev, R. F. Curl, F. K. Tittel, R. Köhler, C. Gmachl, F. Capasso, D. L. Sivco, and A. Y. Cho, "Transportable automated ammonia sensor based on a pulsed thermoelectrically cooled quantum-cascade distributed feedback laser," *Appl. Opt.* **41**, 573–578 (2002).
20. A. A. Kosterev, A. L. Malinovsky, F. K. Tittel, C. Gmachl, F. Capasso, D. L. Sivco, J. N. Baillargeon, A. L. Hutchinson, and A. Y. Cho, "Cavity ringdown spectroscopic detection of nitric oxide with a continuous-wave quantum-cascade laser," *Appl. Opt.* **40**, 5522–5529 (2001).
21. K. A. Cope, M. T. Watson, M. Foster, S. S. Sehnert, and T. H. Risby, "Effects of ventilation on the collection of exhaled breath in humans," *J. Appl. Physiol.* **96**, 1371–1379 (2004).